Sequential pH-Dependent Adsorption of Ionic Amphiphilic Diblock Copolymer Micelles and Choline Oxidase Onto Conductive Substrates: Toward the Design of Biosensors[a]

Larisa V. Sigolaeva,* Ulrike Günther, Dmitry V. Pergushov, Snezhana Yu. Gladyr, Ilya N. Kurochkin, Felix H. Schacher*

This work examines the fabrication regime and the properties of polymer–enzyme thin-films adsorbed onto conductive substrates (graphite or gold). The films are formed via two-steps, sequential adsorption of poly(*n*-butylmethacrylate)-*block*-poly(*N,N*-dimethylaminoethyl methacrylate) (P*n*BMA-*b*-PDMAEMA) diblock copolymer micelles (1st step of adsorption), followed by the enzyme choline oxidase (ChO) (2nd step of adsorption). The solution properties of both adsorbed components are studied and the pH-dependent step-by-step fabrication of polymer–enzyme biosensor coatings reveals rather drastic differences in their enzymatic activities in dependence on the pH of both adsorption steps. The resulting hybrid thin-films represent highly active biosensors for choline with a low detection limit of 30 nM and a good linearity in a range between 30 nM and 100 μM. The sensitivity is found to be 175 μA mM^{-1} cm^{-2} and the operational stability of the polymer–enzyme thin-films can be additionally improved via enzyme-to-enzyme crosslinking with glutaraldehyde.

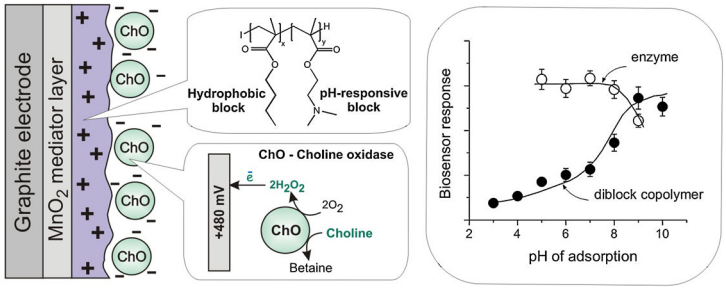

1. Introduction

The efficient immobilization of biomolecules still plays a key role in the research and development of bioanalytical devices like biosensors and biochips. Ideally, most biosensor applications require compact films of the respective biomaterial on a solid substrate, which is strongly attached to the surface. In terms of biomaterial immobilization, electrostatically driven adsorption of proteins onto substrates covered with polyelectrolytes seems to be one of the most straightforward preparation techniques providing controllable amounts and spatial distribution of the

Dr. L. V. Sigolaeva, Dr. D. V. Pergushov, S. Y. Gladyr, Prof. I. N. Kurochkin
Department of Chemistry, Lomonosov Moscow State University, 119991, Moscow, Russia
E-mail: lsigolaeva@genebee.msu.ru

U. Günther, Prof. F. H. Schacher
Institute of Organic and Macromolecular Chemistry, Friedrich-Schiller-University Jena, D-07743, Jena, Germany
E-mail: felix.schacher@uni-jena.de
U. Günther, Prof. F. H. Schacher
Jena Center for Soft Matter (JCSM), Friedrich-Schiller-University Jena, D-07743, Jena, Germany

[a]**Supporting Information** is available from the Wiley Online Library or from the author.

DOI: 10.1002/mabi.201300580

biocatalyst.[1] Polyelectrolytes, when adsorbed to such surfaces, typically exhibit flexible loops and tails of different length, ranging into the solution, and these are capable of accommodating to the shape of protein molecules. Therefore, many theoretical and experimental approaches, as well as industrial efforts, have been focused on electrostatic interactions between proteins and polyelectrolyte-modified charged surfaces, including single-polyelectrolyte or polyelectrolyte-brush layers,[2,3] self-assembled monolayers (SAMs) with charged end groups,[4,5] and polyelectrolyte multilayers (PEMs).[6,7]

Being based on the same principle of electrostatic interactions, layer-by-layer (LbL) assembly techniques are also intensively applied in the field of biosensors.[8] An additional increase in sensitivity of such biosensor elements is usually achieved by the incorporation of nanoparticles and mediators of electron transfer in, for example, multilayer structures.[9–12] However, a nonlinear increase of the analytical response of such sensors with a growing number of layers and/or its decrease after 5–10 layers were reported in many studies.[13,14] These effects are related to a reduced analyte diffusion and electron transport through the layers, which limit the use of multilayer polyelectrolyte/enzyme structures.

Apparently, a bilayer, where an assembly of active enzyme layer is controlled by effective interaction with a pre-adsorbed polyelectrolyte, would represent the ideal structure for a biosensor. Therefore, to our opinion polyelectrolytes can be seen as the crucial interlink between the surface and any enzyme. The amount of incorporated enzyme and the strength of its binding to the respective polyelectrolyte strongly affect basic characteristics of these bioanalytical surfaces, such as activity and operation stability. It is therefore of great interest to develop new types of polyelectrolyte layers.

Another interesting building block for the field of biosensors are polyionic species with nonlinear topology, more precisely star-like micelles formed from amphiphilic (ionic/non-ionic) diblock copolymers in aqueous media.[15] Thereby, the presence of hydrophobic domains might facilitate their adsorption onto relatively hydrophobic substrates while the ionic segments electrostatically bind active enzymes.

The adsorption of diblock copolymer micelles onto planar surfaces has been intensively studied[16–24] for different substrates[25,26] as well as varying adsorption conditions.[27,28] However, such approaches have only rarely been used in the context of biosensor applications. We have recently described the use of such micelles for the polyelectrolyte-induced adsorption of enzymes onto graphite substrates to produce biosensors for phenol and choline, respectively.[29] Based on surface imaging techniques (atomic force microscopy (AFM) and scanning electron microscopy (SEM)), we could demonstrate that the most effective surface coverage of graphite is achieved if the adsorption is carried out in the presence of strong screening counterions for strong polyelectrolytes (charge-suppressed state)[30] or at the respective pH value in case of weak polyelectrolytes.[29] This then led to the subsequent deposition of an increased amount of enzyme and, therefore, higher enzymatic activity of the entire construct.

Nevertheless, clear correlations between the amount of adsorbed material, the charge density of the involved building blocks, and a purposeful variation of the adsorption conditions have not yet been developed.

To understand the underlying processes during polymer–enzyme film formation and the role of electrostatics at any step of the surface modification in more detail, we now expand this to the pH-dependent adsorption of an ionic amphiphilic diblock copolymer, poly(*n*-butylmethacrylate)-*block*-poly(*N,N*-dimethylaminoethyl methacrylate) (P*n*BMA-*b*-PDMAEMA) onto conductive substrates. The subsequent interaction of an electrochemically active enzyme, choline oxidase (ChO), with the diblock copolymer film at different pH values was studied and the effectivity of the polymer–enzyme films as biosensors for choline was assessed. Further, enzyme-to-enzyme crosslinking by glutaraldehyde (GA) was examined as a powerful way to stabilize the resulting biosensor surfaces.

To design our polymer–enzyme biosensor coatings, we applied a graphite-based conductive substrate (screen-printed electrode, SPE), which had been pre-modified by the application of a layer of MnO_2 nanoparticles, serving as mediator for the oxidation of H_2O_2.[31] Afterwards, first a film of the diblock copolymer micelles was attached (Figure 1A, Step 1), followed by washing and drying (Figure 1A, Step 2). Next, the electrochemically active enzyme ChO was adsorbed under different conditions onto the diblock copolymer film (Figure 1A, Step 3). Final washing with water and drying (Figure 1A, Step 4) resulted in biosensor coatings with a high sensitivity to choline. The principle of such a biosensor and its design are also shown in Figure 1. We were particularly interested in i) the charged state of the adsorbing components in solution depending on the pH and ii) the pH-dependent step-by-step fabrication of polymer–enzyme biosensor coatings. Finally, we evaluated the performance of such polymer–enzyme films as biosensors for choline and compared their analytical parameters to already existing setups in the literature.

2. Experimental Section

2.1. Materials

Choline oxidase (ChO) (from *Alcaligenes* sp., E.C. 1.1.3.17, activity 11.6 U mg^{-1}) from Fluka (Germany) was used as electrochemically active enzyme for the preparation of sensor surfaces. Potassium permanganate (Chimmed, Russia) and manganese acetate

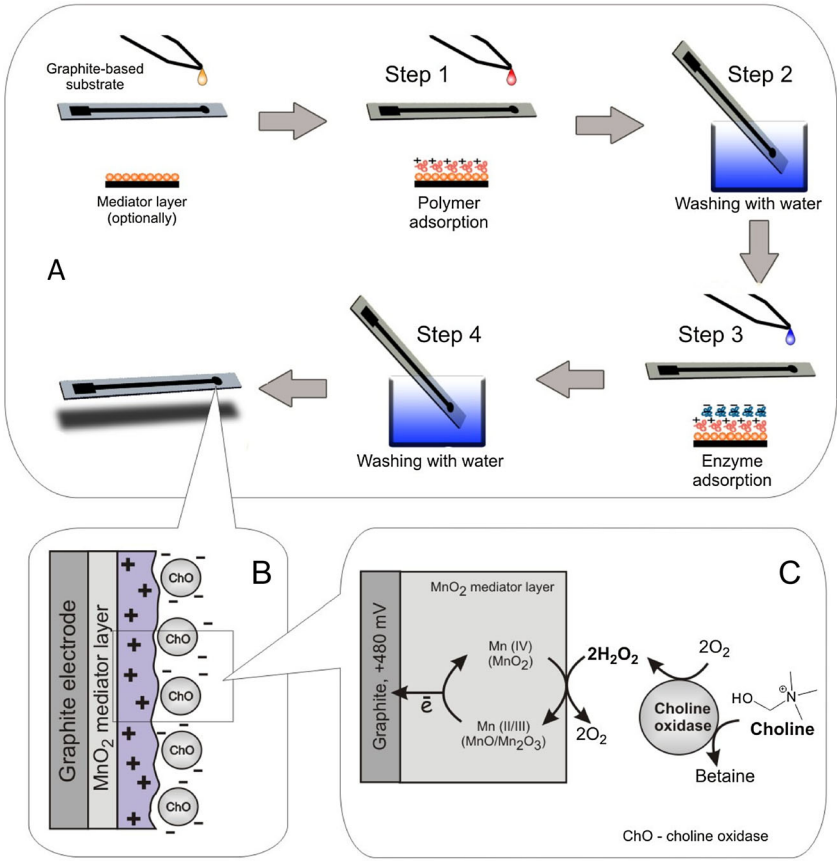

Figure 1. A) Scheme of biosensor preparation. B) Design of the biosensor. C) The underlying principle of the amperometrical detection of choline.

tetrahydrate (Acros, Belgium) were applied for the preparation of manganese dioxide sol solutions. Choline chloride and gluturaldehyde (GA, 25% w/v aqueous solution) were purchased from Sigma–Aldrich. Hydrogen peroxide (30% aqueous solution) was purchased from Fluka (Germany). Phosphate buffer solutions (50 mM PBS) of various pH were prepared by mixing stock solutions of 50 mM NaH_2PO_4 and Na_2HPO_4 and adjusting the pH to the desired value with H_3PO_4 or NaOH. Tris buffer solutions (10 mM tris) of various pH were prepared by mixing stock solutions of 10 mM tris and tris–HCl and adjusting the pH value with HCl. All other chemicals were of analytical grade and used without further purification. All aqueous solutions were prepared using Milli-Q water (18.2 MΩ cm) purified with a Milli-Q water purification system by Millipore.

2.2. Synthesis of P*n*BMA$_{75}$-*b*-PDMAEMA$_{147}$ Diblock Copolymer[32]

To 500 mL of tetrahydrofuran (THF) in a stirred tank reactor 0.2 mL of 1,1-diphenylethylene (DPE, 0.198 g, 1.1 mmol) and 0.71 mL of *sec*-butyllithium (*s*-BuLi, 1 mmol) were added at −78 °C to form the initiating system, 1,1-diphenylhexyllithium (DPHLi). Afterwards, 10.1 mL of *n*-butyl methacrylate (*n*BMA, 9 g, 63.3 mmol) were added with a syringe. The mixture was then slowly warmed to −50 °C and held at that temperature for 1 h. *N*,*N*-Dimethylaminoethyl methacrylate (DMAEMA, 22.6 mL, 21 g, 133.7 mmol) was then added with a syringe and polymerized at the same temperature for another hour. The reaction was quenched by the addition of 2 mL of degassed isopropyl alcohol. The polymer was purified by dialysis (MWCO 8 000 g mol^{-1}) against dioxane and dioxane/water 80/20 mixtures to remove the Li^+ and freeze-dried afterwards. Characterization according to ^{1}H NMR spectroscopy and size exclusion chromatography (SEC) gave a number-average molecular weight of 10 600 g mol^{-1} for the P*n*BMA block and 23 100 g mol^{-1} for the PDMAEMA block. The polymer is denoted as PnBMA$_{75}$-*b*-PDMAEMA$_{147}$ (subscripts denoting the respective degrees of polymerization) with an overall number-average molecular weight of 33 700 g mol^{-1} and a polydispersity index (PDI) of 1.10.

2.3. Potentiometric Titration

Potentiometric titration of P*n*BMA$_{75}$-*b*-PDMAEMA$_{147}$ was performed using a digital pH meter (Orion) equipped by combined glass/reference electrode, calibrated with standard buffer solutions of pH 4.0, 7.0, and 10.0 (Oacton, Orion). The titration of P*n*BMA$_{75}$-*b*-PDMAEMA$_{147}$ was started from the initial pH value of diblock copolymer aqueous solution with the concentration of 0.005 M in monomeric units. 10 mM HCl was used as the titrant, which was added by 10 μL portions to a 1.5 mL sample of diblock copolymer solution at a constant temperature (25 °C) and under intensive stirring. pH readings were registered after establishing the equilibrium state when the pH reached a constant value after each step of titrant addition. The degree of protonation of the tertiary amino group α was calculated as the molar ratio of the added titrant to the PDMAEMA monomer units. For the calculation of the pK_a values, the Henderson–Hasselbalch equation was used.

2.4. Quartz Crystal Microbalance with Dissipation Monitoring (QCM-D)

The adsorption of diblock copolymer micelles and enzyme was followed in situ by QCM-D (Q-Sense, E1 system). The sensor crystals (Q-Sense) are AT-cut quartz with gold-plated polished electrodes. The quartz crystals were excited at their fundamental frequency ($f_0 \approx 5$ MHz) as well as at the 3rd, 5th, 7th, 9th, and 11th overtones, corresponding to 15, 25, 35, 45, and 55 MHz, respectively. Before use, the crystals were cleaned according to the Q-Sense cleaning protocol by sequential ozone treatment for 10 min, then treatment by a mixture of Milli-Q water/NH_4OH/H_2O_2 = 5:1:1 at 70 °C for 10 min, followed by rinsing with Milli-Q water, blowing by air flux, and again ozone treatment for 10 min. Before the adsorption

experiments, the sensors were premodified by a MnO_2 layer via spray-coating of the MnO_2 nanoparticle solution. Each sensor was fixed at the angle of 45° to the head of a home-made spraying injector and the MnO_2 aerosol was sprayed onto an active sensor area from a distance of 20 cm. After spraying of each layer, the sensor was allowed to dry completely. This procedure was repeated 15 times for each sensor. Then the modified sensors were washed with Milli-Q water and any excess water was removed by air flux. Each QCM-D experiment was started from baseline recording for the 50 mM PBS at the corresponding pH value. Then the P*n*BMA$_{75}$-*b*-PDMAEMA$_{147}$ micelles were first adsorbed (from 10 g L^{-1} solutions in the same buffer at the corresponding pH value), followed by a washing step with the initial buffer to remove any loosely attached material. After this assembly step, the QCM sensors were withdrawn from the Q-Sense flow-through cell, washed thoroughly with Milli-Q water and dried by a stream of air (in the same way as for SPEs). For enzyme adsorption studies, ChO (4 g L^{-1} in a 10 mM tris at the corresponding pH value) was deposited on the pre-adsorbed layer of the diblock copolymer in the same way. Thereafter, a protein-free 10 mM tris solution of the same pH was used to remove weakly adsorbed protein molecules. During each adsorption stage, frequency and dissipation shifts were continuously recorded as a function of time. For all experiments, the temperature was set to 25 °C. Each study was performed in duplicate. Data analysis was carried out using the viscoelastic Voigt-based model of the integrated QTools software provided with the QCM-D equipment. The masses of the wet films were calculated separately for each adsorption stage by fitting the QCM-D data regarding the 3th, 5th, 7th, 9th, and 11th overtones.

2.5. ζ-Potential Measurements

The ζ-potentials were measured on a ZetaSizer Nano ZS from Malvern via the M3-PALS technique with a laser operating at $\lambda = 633$ nm. The detection angle was 17°. The electrophoretic mobilities (u) were converted into ζ-potentials via the Henry equation $\zeta = u\eta/\varepsilon_0\varepsilon$ in the Smoluchowski approximation, where η denotes the viscosity and $\varepsilon_0\varepsilon$ the permittivity of the solution. For ζ-potential measurements of P*n*BMA$_{75}$-*b*-PDMAEMA$_{147}$ micelles, the diblock copolymer solutions were prepared in 50 mM PBS (pH 3–10) at a concentration of 0.2 g L^{-1}. For ζ-potential measurements of ChO, the enzyme solutions were prepared in 10 mM tris (pH 5–9) at a concentration of 1 g L^{-1}. Prior to any solution preparation, the buffers were filtered three times trough nylon filters (Target Thermo Fisher Scientific Inc.) with a pore size of 0.2 μm. The enzyme solutions were additionally filtered three times through nylon filters (Target Thermo Fisher Scientific Inc.) with a pore size of 1.4 μm. The samples were measured in folded capillary cells from Malvern. The measurements were performed at 25 °C at least in triplicate and results are given as mean ± SD.

2.6. Dynamic Light Scattering (DLS)

DLS measurements were performed on an ALV CGS-3 setup equipped with a He—Ne laser operating at a wavelength of $\lambda = 632.8$ nm and at a scattering angle of 90°. The CONTIN algorithm was applied to analyze the obtained correlation functions. In all cases, the diblock copolymer stock solutions were diluted with 50 mM PBS (pH 3–10) to a final concentration of 0.2 g L^{-1}. Prior to any solution preparation, the buffers were filtered three times through nylon filters (Target Thermo Fisher Scientific Inc.) with a pore size of 0.2 μm.

2.7. Contact Angle (CA) Measurements

Static CAs on flat substrates were derived from drop shape analysis on an OCA 30 from DataPhysics Instruments GmbH, Germany at room temperature. CAs were measured with Milli-Q water as a probe liquid. A drop of 2.5 μL was automatically placed on the SPE substrate covered by the film studied. Measurements were performed immediately after drop deposition to avoid water evaporation. The CA measurements were repeated six to eight times on different locations and the values were subsequently averaged.

2.8. Cryogenic Transmission Electron Microscopy (cryo-TEM)

For cryo-TEM, 5 μL of the sample solution were applied to copper grids covered with a holey carbon film (Quantifoil R3.5/1 Micro Tools GmbH, Jena, Germany). The excess of the solution was automatically blotted with a filter paper (1 s), and the grid was then plunged rapidly into liquid ethane (−180 °C) in a cryo-box (Carl Zeiss NTS GmbH). After removing excess ethane with a filter paper, the samples were transferred with a cryo-transfer unit (Gatan 626-DH, Gatan GmbH, Münich, Germany) into the pre-cooled cryo-electron microscope operated at 120 kV (Philips CM 120, Eindhoven, The Netherlands) and viewed under low dose conditions with a bottom-mounted 1k CCD camera. Images were processed with a UTHSCSA Image Tool 3.00.

2.9. Polymer–Enzyme Film Assembly

For an electrochemical enzymatic activity assay of the polymer–enzyme films, the SPEs were fabricated on poly(vinyl chloride) substrates of 0.2 mm thickness by means of conductive graphite paste (Gwent, UK) screen-printed by a semiautomated Winon machine (model WSC-160B, China) with a 200 mesh screen stencil. Each SPE consisted of a round-shaped working area (2.5 mm diameter), a conductive track (30 mm × 1.5 mm), and a square extremity (3 mm × 7 mm) for electrical contact. Before adsorption of the diblock copolymer and the enzyme, all SPEs were premodified by a peroxide-sensitive MnO_2 layer according to a published protocol.[31] Shortly, a freshly prepared MnO_2 sol solution was formed via 1:1 mixing of 0.25 mM $KMnO_4$ and 0.375 mM of $Mn(CH_3COO)_2$ and shaking for 5 min. Then the working area of each SPE was covered by a 10 μL drop of the MnO_2 sol solution, followed by complete drying at room temperature for ca. 2–2.5 h, rinsing with Milli-Q water, and heating at 60 °C for 1 h. The modified SPEs were stored dry at ambient temperature until further use. The 10 g L^{-1} solutions of P*n*BMA$_{75}$-*b*-PDMAEMA$_{147}$ micelles were prepared in pH 3–10 PBS buffers by direct dissolution of the diblock copolymer with intensive stirring for 5–7 d at ambient

temperature. When lower concentrations were necessary, they were prepared by a direct dilution of stock solutions with the same buffer media. ChO was prepared in 4 g L^{-1} concentration in 10 mM tris with a desired pH value in the range of pH 5–9 immediately before experiments. The micelles were adsorbed onto SPEs by covering the working area of each SPE by a 10 μL drop of the P*n*BMA$_{75}$-*b*-PDMAEMA$_{147}$ solution, followed by 1 h adsorption. After that time, the substrate was rinsed with Milli-Q water and dried using a stream of air. The enzyme was adsorbed in a similar way for 10 min, followed by rinsing with Milli-Q water and drying with a stream of air. To prevent loss of enzymatic activity, SPEs modified by polymer–enzyme films were stored at +4 °C until further use. The design and the measurement principle of the P*n*BMA$_{75}$-*b*-PDMAEMA$_{147}$/ChO biosensors is shown in Figure 1.

2.10. Electrochemical Assay of ChO Activity

Electrochemical experiments were performed at ambient temperature in a one-compartment electrochemical cell under stirring (volume of 1 mL) using a two-electrode configuration. The SPE covered by a polymer–enzyme film with an active surface area of 0.049 cm^2 served as the working electrode and Ag/AgCl (with length of 1 cm, diameter of 3 mm, and surface area of 1.03 cm^2) was used as a reference electrode. A micro-potentiostate IPC-Micro (Kronas Ltd., Russia) used for electrochemical measurements was connected to a computer and electrochemical parameters were controlled by using a micro-potentiostate software. The amperometrical responses for choline for ChO-containing films were measured in 50 mM HEPES buffer with 30 mM KCl (pH 7.5), by recording a current arising in response to the addition of substrate. This oxidative current is generated due to H_2O_2 oxidation (mediated by MnO_2) at an applied potential (+480 mV vs Ag/AgCl) and is directly proportional to the amount of choline added and the ChO activity as well (Figure 1C). The analytical signal for choline of the enzyme-based electrode was determined as a value of steady-state baseline current change (the difference between an average value of steady-state baseline current before and after choline addition). Each electrochemical result is presented as mean ± SD calculated from at least three sensor responses obtained for at least three different electrodes. To stabilize the sensors by cross-linking with GA, the SPEs coated with P*n*BMA$_{75}$-*b*-PDMAEMA$_{147}$/ChO films were dipped in aqueous 1% w/v solution of GA for 60 min, followed by rinsing thoroughly for 1–2 min with Milli-Q water, after which the sensors were stored under air at +4 °C until further use.

2.11. Spectrophotometric Assay of ChO Activity

The ChO activity was further assayed in 96-well microplates using a microtiter plate reader Antos HT1 (Austria) according to a protocol described in the literature.[33] Each well was filled with 250 μL of reagent mixture containing 0.14 mM of choline chloride; 0.48 mM of 4-amino-antipurine; 2.1 mM of phenol, and 5 mU of horse radish peroxidase diluted in 10 mM tris buffer (pH 8.0). The enzymatic reaction was started by the addition of a 20 μL aliquots of ChO from stock solutions preincubated at specified time periods in 10 mM tris buffers with pH ranged from 3 to 9. The appearance of colored product was measured at λ = 492 nm in five cycles with 20 s duration. The ChO activity was assumed to be proportional to the increase in the absorbance of the samples with time and it was expressed as mAbs min^{-1}.

3. Results and Discussion

3.1. P*n*BMA$_{75}$-*b*-PDMAEMA$_{147}$ Solution Properties and Adsorption

In this study, we used an amphiphilic diblock copolymer, poly(*n*-butylmethacrylate)-*block*-poly(*N*,*N*-dimethylaminoethyl methacrylate), P*n*BMA$_{75}$-*b*-PDMAEMA$_{147}$, where the subscripts denote the corresponding number-average degrees of polymerization of the corresponding blocks and with a molecular weight of 33 700 g mol^{-1} (PDI = 1.10). The chemical structure of the diblock copolymer is shown in Figure 2A. P*n*BMA$_{75}$-*b*-PDMAEMA$_{147}$ comprises both a hydrophobic P*n*BMA (with a moderately low T_g)[34] and a hydrophilic PDMAEMA block (depending on the solution pH and the temperature). In aqueous media, P*n*BMA$_{75}$-*b*-PDMAEMA$_{147}$ forms micelles with a P*n*BMA core and a PDMAEMA corona, most presumably of star-like

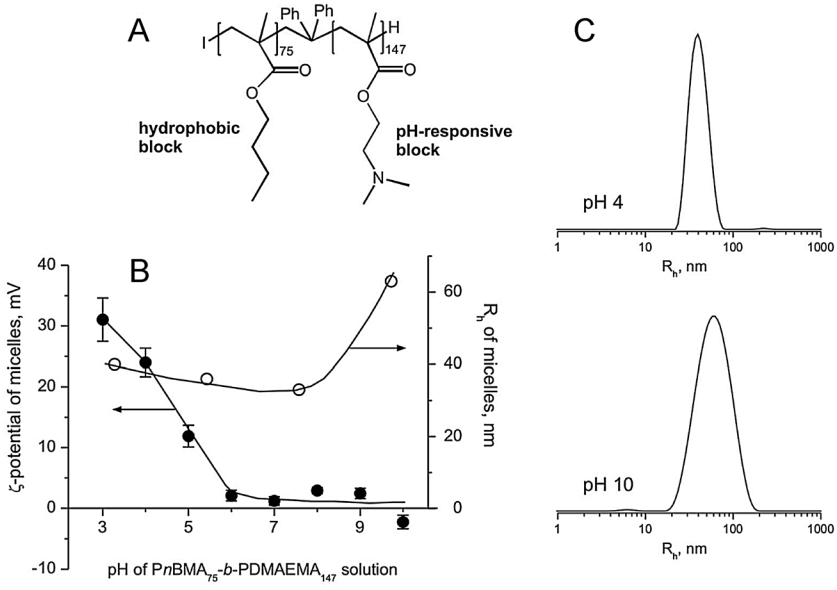

Figure 2. A) Chemical structure and B) ζ-potentials for P*n*BMA$_{75}$-*b*-PDMAEMA$_{147}$ micelles (solid circles) as well as the corresponding hydrodynamic radii R_h (open circles) (0.5 g L^{-1} in 50 mM PBS with pH in the range of 3–10). C) DLS CONTIN plots at pH 4 (R_h = 40 nm) and pH 10 (R_h = 63 nm).

type. As PDMAEMA is a weak polyelectrolyte, the charge and the solution structure (e.g., corona extension) of these micelles is pH-dependent. To understand the effect of the pH, both the size and the charge of P*n*BMA$_{75}$-*b*-PDMAEMA$_{147}$ micelles were investigated by dynamic light scattering (DLS) and ζ-potential measurements.

DLS data on hydrodynamic radii of P*n*BMA$_{75}$-*b*-PDMAEMA$_{147}$ micelles are given in Fig. 2B, together with the corresponding intensity-weighted DLS CONTIN plots for pH 4 and 10 (Figure 2C). More DLS results are given in the SI (Figure S1, Supporting Information). Monomodal size distributions are obtained at all pH values, hinting toward rather well-defined structures. As shown in Figure 2B, individual micelles composed from P*n*BMA$_{75}$-*b*-PDMAEMA$_{147}$ (contour length is 55.5 nm) exhibit a hydrodynamic radius of $R_h = 40$ nm at pH 4, which slightly decreases to $R_h = 33$ nm if the pH increases to 8. This can be explained by the pH-responsive behavior of PDMAEMA: the chains are highly stretched at low pH but become less charged with increasing pH as the degree of protonation of the PDMAEMA chains decreases. A nearly twofold increase in the R_h can be observed at pH 10 ($R_h = 63$ nm) and can be ascribed to a certain aggregation of the micelles occurring.[29] The core–corona structure of the micelles was additionally visualized by cryogenic transmission electron microscopy (cryo-TEM) according to which the micellar cores are seen at pH 7 as spherical objects of uniform size with a mean diameter of 22 ± 3 nm (averaged value was obtained from approximately 70 micelles (Figure S2, Supporting Information)). The water-soluble PDMAEMA corona is not visible in the cryo-TEM micrograph due to its low electron density. The size of the micellar core found for P*n*BMA$_{75}$-*b*-PDMAEMA$_{147}$ fits very well to small-angle neutron scattering data reported by Burkhardt et al.[35] for polyisobutylene-*block*-poly(methacrylic acid) (PIB$_{75}$-*b*-PMAA$_{190}$) with comparable lengths of the hydrophobic ($\overline{DP}_n = 75$) and the ionic ($\overline{DP}_n = 190$) block. The authors found $R_{core} = 8.7$ nm ($\alpha = 1$) and $R_{core} = 12.4$ nm ($\alpha = 0.1$) depending on the ionization degree α of PMAA block. This supports our evaluation of the core size ($R_{core} = 11$ nm) for P*n*BMA$_{75}$-*b*-PDMAEMA$_{147}$ micelles.

The corresponding ζ-potentials of the micellar structures at different pH are shown in Figure 2B. This data also confirms the pH-sensitive behavior of PDMAEMA. At pH 3, highly positively charged micelles in PBS exhibit a ζ-potential of about +30 mV, whereas the value decreases and becomes nearly zero at pH 6. No more changes in the ζ-potentials were observed upon further increase in pH.

This pH-dependent charge characteristics of the P*n*BMA$_{75}$-*b*-PDMAEMA$_{147}$ micelles allow us to predict their interactions with a hydrophobic solid interphase. Deprotonation of the PDMAEMA segments together with effective PDMAEMA charge screening induced by the presence of phosphate counterions (from PBS) will obviously shift PDMAEMA into the non-charged state at pH $\geq$6 and should facilitate the drift of such micelles from the water phase to the solid support. Therefore, higher adsorption of diblock copolymer micelles is expected to occur at pH $\geq$6.

To verify our assumptions (Figure 1A, Step 1), the pH-dependent adsorption of P*n*BMA$_{75}$-*b*-PDMAEMA$_{147}$ was studied using a quartz crystal microbalance with dissipation monitoring (QCM-D), a technique that is suitable for adsorption studies of soft viscoelastic films on a piezoelectric quartz crystal. This technique allows simultaneous in situ measurements of a layer resonance frequency, f, and dissipation, D, at several overtones of the fundamental frequency. Afterwards, f and D data modeling according to the viscoelastic model by Voigt[36] correctly evaluates the adsorbed mass (or thickness) of soft films along with other viscoelastic properties like layer viscosity and shear modulus. In our QCM-D experiments, P*n*BMA$_{75}$-*b*-PDMAEMA$_{147}$ was adsorbed onto gold-coated quartz crystals, pre-modified with a spray-coated layer of MnO_2 nanoparticles. This has been done in order to mimic the surface of the otherwise employed SPEs, which are covered by a similar mediator layer of MnO_2 nanoparticles. The diblock copolymer solutions were prepared in 50 mM PBS (pH 3–9) at a concentration of 10 g L^{-1}, the same buffer conditions were used as shown earlier for ζ-potential measurements. The frequency (Δf) and dissipation changes (ΔD) during P*n*BMA$_{75}$-*b*-PDMAEMA$_{147}$ adsorption obtained at overtone numbers of $n = 3, 5, 7, 9$, and 11 were recorded as a function of time. As was found, each case of polymer adsorption corresponds to a decrease of Δf and an increase of ΔD with the spreading of overtones (data not shown here), which denotes that the mass deposited onto the crystal surface exhibits viscoelastic properties. Then, a rinsing step was performed in order to confirm that both the changes in Δf and ΔD are not the result of variations in the solution properties, such as density and viscosity. By fitting the QCM-D data, it was possible to estimate the mass variation as a function of the pH. Figure 3 presents the effect of the pH of the P*n*BMA$_{75}$-*b*-PDMAEMA$_{147}$ solution on the mass of adsorbed material together with associated water. It is clearly seen that the mass of the hydrated polymer layer considerably increases with the pH and this effect is opposite to the ζ-potential of the micelles determined in the same buffer media (compare with Figure 2B). Moreover, the higher the pH of adsorption, the higher was the ratio of the diblock copolymer/water in the adsorbed layer, presumably due to deprotonation of the PDMAEMA corona, accompanied by an increase in hydrophobicity of the whole system. Thus, the formation of P*n*BMA$_{75}$-*b*-PDMAEMA$_{147}$ films at higher pH results in a higher mass of the adsorbed diblock copolymer due to an increasing affinity of the micelles to a MnO_2 premodified crystal. These data are in a good agreement

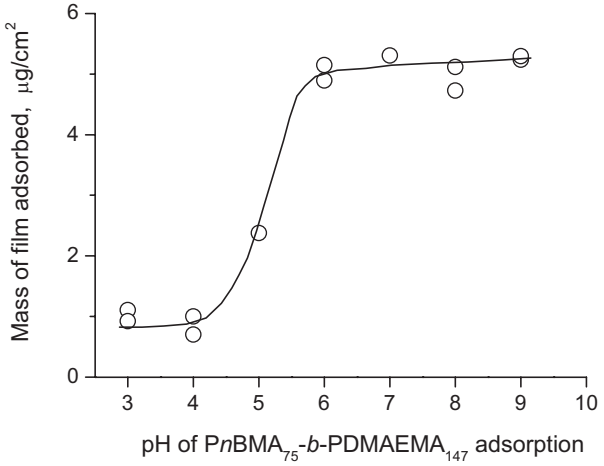

Figure 3. Mass of the hydrated film of P*n*BMA$_{75}$-*b*-PDMAEMA$_{147}$ adsorbed in the pH-range of 3–9. Conditions: gold-coated QCM quartz crystals premodified by MnO_2 nanoparticles via spray-coating, the diblock copolymer micelles were adsorbed from 10 g L^{-1} solutions in 50 mM PBS in the pH-range 3–9. Lines through the experimentally derived data points are drawn only as a guide to the eye.

with AFM characterization of highly oriented pyrolytic graphite modification with poly(butadiene)-*block*-poly(*N*,*N*-dimethylaminoethyl methacrylate)[29] or poly-(diallyldimethylammonium chloride).[30]

The next step was to remove any weakly adsorbed molecules and salts by washing, followed by drying in the air to stabilize the whole film and to improve its attachment to the substrate (see Figure 1A, Step 2). It can be assumed that most of the phosphate counterions are rinsed off the P*n*BMA$_{75}$-*b*-PDMAEMA$_{147}$ layer and this might affect the charge conditions of the PDMAEMA blocks. This was assessed by potentiometric titration of an aqueous P*n*BMA$_{75}$-*b*-PDMAEMA$_{147}$ solution. As PDMAEMA is a weak polyelectrolyte, its titration by HCl solution results in the complete protonation of the ternary amino group (Figure 4). Assuming α as the protonation degree of the PDMAEMA block (see also the description given in Figure 4) and determining $\alpha = 0$ at the initial pH of the diblock copolymer solution and $\alpha = 1$ at the point of inflection of the curve (pH vs *V* of titrant added), one can plot the dependence of the protonation degree α of the PDMAEMA block on the pH (α vs pH) (Figure 4). According to this dependence, the pH-sensitive PDMAEMA block in P*n*BMA$_{75}$-*b*-PDMAEMA$_{147}$ undergoes a conversion from the fully protonated (charged) state to the fully deprotonated (non-charged) condition in between the pH range of about 5.5–8.5. Although these values refer to the solution state of the PDMAEMA block, we assume that they can be extended to the adsorbed state of P*n*BMA$_{75}$-*b*-PDMAEMA$_{147}$ as well and are beneficial for the understanding of the following enzyme adsorption (Figure 1A, Step 3).

The data on the pK_a^{char} ($\alpha = 0$) and pK_a^{app} ($\alpha = 0.5$) for P*n*BMA$_{75}$-*b*-PDMAEMA$_{147}$ determined according to the Henderson–Hasselbalch equation are summarized in Table 1. The value of $pK_a^{app} = 6.37$ ($\alpha = 0.5$) was found to be in good agreement with pK_a^{app} ($\alpha = 0.5$) found for star-shaped PDMAEMAs[37,38] and comparable with the values of pK_a^{app} ($\alpha = 0.5$) found for other linear and star-shaped PDMAEMAs.[39,40]

As the following enzyme adsorption will take place under different buffer conditions, which have proven favorable for preserving the specific enzymatic activity of ChO (typically in 10 mM tris), the potentiometric titration of P*n*BMA$_{75}$-*b*-PDMAEMA$_{147}$ was also carried out in the presence of 100 mM NaCl to clarify the effect of salt on the degree of protonation of the PDMAEMA block in P*n*BMA$_{75}$-*b*-PDMAEMA$_{147}$. The corresponding curves of (pH vs. *V* of titrant added), (α vs. pH), and also pK_a values are also given in Figure 4 and Table 1, respectively. The expected increase in pK_a found in the presence of salt can be easily explained by the fact that salt always stabilizes the protonated form, otherwise the presence of salt will shift the equilibrium in the reaction $-N(CH_3)_2H^+ \leftrightarrows -N(CH_3)_2 + H^+$ towards $-N(CH_3)_2H^+$. This

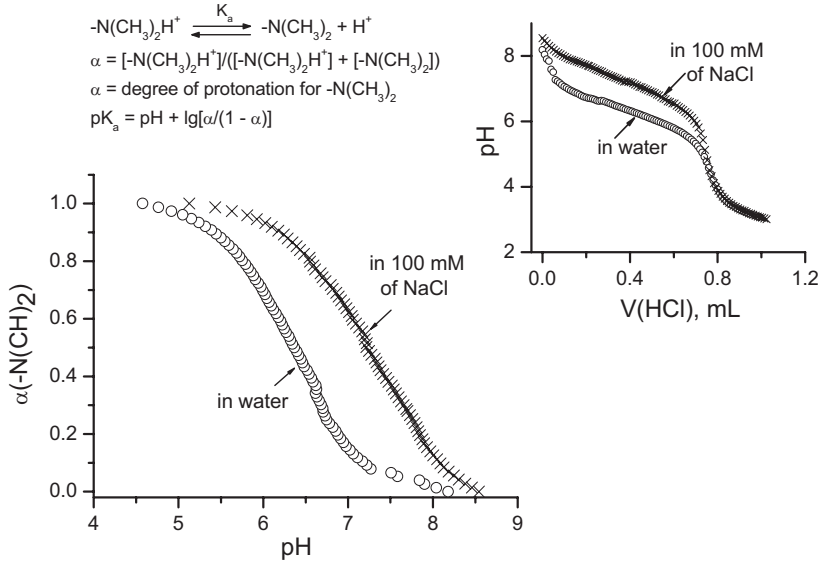

Figure 4. Dependence of the protonation degree α of the PDMAEMA block on the pH in water and in the presence of 100 mM NaCl. Inset: initial potentiometric titration curves of P*n*BMA$_{75}$-*b*-PDMAEMA$_{147}$. The diblock copolymer concentration was 5 mM (in terms of the concentration of ionic groups of the PDMAEMA block). The titration was started from pH 8.18 (in water) or from pH 8.54 (in 100 mM of NaCl) and was performed by stepwise addition of 10 μL of 10 mM HCl.

Table 1. pK_a values for —$N(CH_3)_2$ group for various PDMAEMA samples in aqueous solutions.

Polymer sample	Conditions	pK_a^{char} ($\alpha = 0$)[a)]	pK_a^{app} ($\alpha = 0.5$)	Refs.
P*n*BMA$_{75}$-*b*-PDMAEMA$_{147}$	In water	6.40	6.37	This work
P*n*BMA$_{75}$-*b*-PDMAEMA$_{147}$	100 mM of NaCl	7.40	7.23	This work
Star-shaped (PDMAEMA$_{235}$)$_{19.5}$	In water		6.73	[37]
Star-shaped (PDMAEMA$_{100}$)$_3$	In water		6.70	[38]

[a)] pK_a^{char} ($\alpha = 0$) values were determined according to the Henderson–Hasselbalch equation from a plot of $[pK_a = pH + lg[\alpha/(1-\alpha)]$ vs. $\alpha]$. pK_a^{char} ($\alpha = 0$) values were obtained by applying limiting conditions $0.15 < \alpha < 0.9$ and extrapolating to $\alpha = 0$.

results in the decrease of K_a or the increase of the $pK_a = -lg\, K_a$.

To get insight into the surface characteristics of the resulting P*n*BMA$_{75}$-*b*-PDMAEMA$_{147}$ films in the dry state, contact angle (CA) measurements were carried out (Table 2). The adsorption of P*n*BMA$_{75}$-*b*-PDMAEMA$_{147}$ micelles onto the SPE notably decreases the CA (CA for SPE = 133.3 ± 0.8 or SPE/MnO_2 131.6 ± 0.7), indicating a successful surface modification. However, the CAs of the resulting P*n*BMA$_{75}$-*b*-PDMAEMA$_{147}$ films appear to be nearly independent of the pH during adsorption. Only a slight increase in CA is observed in the alkaline region.

3.2. ChO Solution Properties and Adsorption

To understand the next step (pH-dependent adsorption of ChO, Figure 1A, Step 3), the net charge of ChO should be characterized at different pH values. As the isoelectric point (IEP) of ChO is reported to be 4.1 ± 0.1,[33] ChO apparently is negatively charged at pH > IEP. To confirm this as well as to examine the trend of net negative charge of ChO versus pH, the ζ-potentials of ChO in 10 mM tris have been evaluated at different pH (5–9). The lower limit of this pH-range is 5 as ChO is irreversibly inactivated in acidic media at pH ≤4 (see Figure S3, Supporting Information, showing the pH stability of ChO in solution). As can be seen in Figure 5, the ChO molecules bear a net negative charge over the whole pH range investigated, which is in agreement with the reported IEP. Only small changes in ζ-potential were found with increasing pH (from −18.3 ± 0.9 mV for pH 5 to −26.5 ± 1.6 mV for pH 9). Therefore, strong electrostatic interactions between the enzyme and P*n*BMA$_{75}$-*b*-PDMAEMA$_{147}$ can be expected, provided the latter still being positively charged under these conditions.

Considering the electrostatic complexation of ChO with the layer of the pre-adsorbed diblock copolymer (Figure 1A, Step 3), we have to distinguish two different situations. First, the pH during diblock copolymer adsorption is varied, whereas the pH during enzyme adsorption is kept constant. Second, vice versa, the diblock copolymer

Table 2. Contact angles (CA) for diblock copolymer and diblock copolymer–enzyme films adsorbed onto SPE.

	Static CA (mean ± SD, n = 6–8)	
pH of polymer adsorption	P*n*BMA$_{75}$-*b*-PDMAEMA$_{147}$ film	P*n*BMA$_{75}$-*b*-PDMAEMA$_{147}$/ChO film
3	88.5 ± 5.4	67.2 ± 3.0
4	83.9 ± 5.2	75.0 ± 2.6
5	89.0 ± 4.7	78.1 ± 4.0
6	78.1 ± 5.7	65.2 ± 0.8
7	89.2 ± 2.8	56.1 ± 2.0
8	91.4 ± 2.9	51.5 ± 2.1
9	97.3 ± 3.1	47.8 ± 2.8
10	96.3 ± 3.0	43.5 ± 2.6

Conditions: the diblock copolymer was adsorbed at a concentration of 10 g L^{-1} in the pH range 3–10 for 1 h, the enzyme was adsorbed at a concentration of 1 g L^{-1} at pH 7 for 10 min. CA values for the naked SPE and SPE covered by MnO_2 were found to be 133.3 ± 0.8 and 131.6 ± 0.7, respectively.

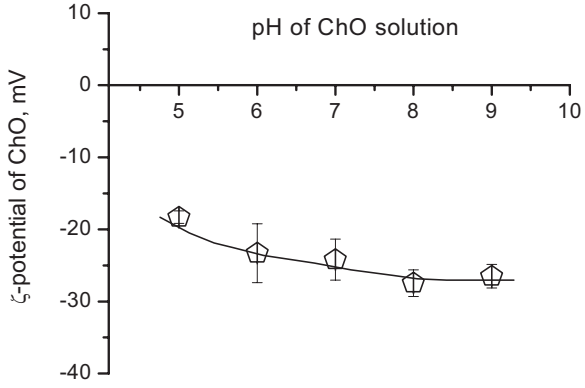

Figure 5. ζ-potentials of ChO (1 g L^{-1} in 10 mM tris with pH in the range of 5–9).

adsorption occurs at constant pH, but during enzyme adsorption different pH values are used.

Regarding both situations, we examined the ChO adsorption by QCM-D onto the MnO_2-treated gold-coated quartz crystals covered by pre-adsorbed P*n*BMA$_{75}$-*b*-PDMAEMA$_{147}$. The enzyme solutions were prepared at a concentration of 4 g L^{-1} in 10 mM tris at different pH (5–9). The adsorption of enzyme also induces a decrease of Δf and an increase of ΔD, although with less spreading of overtones (data not shown here), which denotes that the enzyme film appears more rigid in comparison to the diblock copolymer film. Fitting of the QCM-D data has been done for one layer film again in accordance to the viscoelastic model by Voigt,[36] allowing us to estimate the mass of the enzyme layer as a function of the pH of P*n*BMA$_{75}$-*b*-PDMAEMA$_{147}$ pre-adsorption (Figure 6A) or as a function of the pH of the enzyme adsorption (Figure 6B).

Figure 6A depicts experiments where a series of QCM sensors has been covered by P*n*BMA$_{75}$-*b*-PDMAEMA$_{147}$ at different pH. Their subsequent interaction with ChO was studied at pH 7, which corresponds to a protonation degree of about 50% for P*n*BMA$_{75}$-*b*-PDMAEMA$_{147}$, according to the potentiometric titration results (Figure 4). Our data clearly shows that the mass of the hydrated enzyme film considerably increases if P*n*BMA$_{75}$-*b*-PDMAEMA$_{147}$ was deposited at pH >7. This seems to be a consequence of an increased diblock copolymer adsorption, which, as it was found, takes place in the same pH range (Figure 3). The pH-dependent increase in the amount of enzyme adsorbed is the result of a higher surface coverage by P*n*BMA$_{75}$-*b*-PDMAEMA$_{147}$ due to an increasing surface affinity of the diblock copolymer if the PDMAEMA segment carries a lower amount of charges.

The increased adsorption of enzyme was additionally confirmed by CAs measured for P*n*BMA$_{75}$-*b*-PDMAEMA$_{147}$/ChO films on SPEs (Table 2). A notable monotonous decrease in CA values was observed at pH ≥6 (starting from 65.2 ± 0.8 for pH 6 and coming to 43.5 ± 2.6 for pH 10) hinting toward a more hydrophilic film surface and, hence, an increased amount of adsorbed enzyme.

Alternatively, Figure 6B shows a series of experiments with QCM sensors premodified by deposition of P*n*BMA$_{75}$-*b*-PDMAEMA$_{147}$ at pH 9. Their subsequent interaction with ChO was studied at pH varied from 5 to 9. Our data suggests that an almost constant mass of hydrated enzyme film is formed at pH 5–8. Notable decrease in the mass was only found for pH 9. If one compares this data to the plot for the pH-dependent protonation degree of the PDMAEMA block (Figure 4) and with ζ-potentials for ChO (Figure 5), the conclusion can be drawn that rather the presence than the actual amount of positive charges is crucial during enzyme adsorption. Only when the PDMAEMA block becomes nearly uncharged, electrostatically driven adsorption of the enzyme is suppressed. This explains why a decreased mass of the ChO-containing film was observed at pH 9 where P*n*BMA$_{75}$-*b*-PDMAEMA$_{147}$ is almost completely deprotonated and uncharged. Only non-electrostatic (most probably hydrophobic) interactions can be realized under these conditions. At the same time, the appearance of only small amounts of positive charges at pH 8 results in a considerable increase in the amount of the enzyme adsorbed. Similar observations are reported in other studies[41–44] on the interaction of proteins with oppositely and similarly charged polyelectrolyte species.

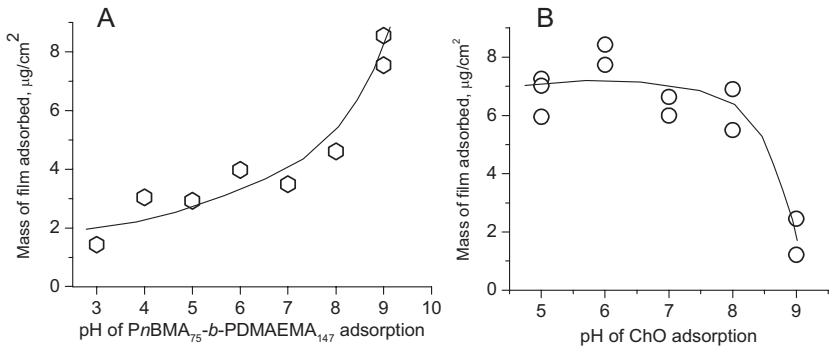

Figure 6. Mass of hydrated ChO film adsorbed depending on A) the pH of P*n*BMA$_{75}$-*b*-PDMAEMA$_{147}$ pre-adsorption and B) depending on the pH of ChO adsorption. Conditions for (A): ChO adsorption was carried out from 4 g L^{-1} solution in 10 mM tris (pH 7) onto gold-coated QCM quartz crystal premodified by MnO_2 and covered by a P*n*BMA$_{75}$-*b*-PDMAEMA$_{147}$ film pre-adsorbed from 10 g L^{-1} solutions of the material in 50 mM PBS (pH 3–9). Conditions for (B): ChO adsorption was carried out from 4 g L^{-1} solutions in 10 mM tris in the range of pH 5–9 onto gold-coated QCM quartz crystal premodified by MnO_2 and covered by a P*n*BMA$_{75}$-*b*-PDMAEMA$_{147}$ film pre-adsorbed from 10 g L^{-1} solution in 50 mM PBS (pH 9). Lines through the experimentally derived data points are drawn only as a guide to the eye.

3.3. Enzymatic Activity and Stability of the Biosensor Coating

In addition to QCM-D experiments, the enzymatic activities of the polymer–enzyme films were tested. Specific enzymatic activities of the P*n*BMA$_{75}$-*b*-PDMAEMA$_{147}$/ChO films deposited onto MnO_2 premodified SPE surfaces were determined amperometrically as response of the system to the addition of a standard choline concentration (the detailed measuring principle is described in Figure 1). Similarly to the performed QCM-D studies, the activity of the resultant ChO-containing films was examined both as a function of the pH of P*n*BMA$_{75}$-*b*-PDMAEMA$_{147}$ deposition and the pH of

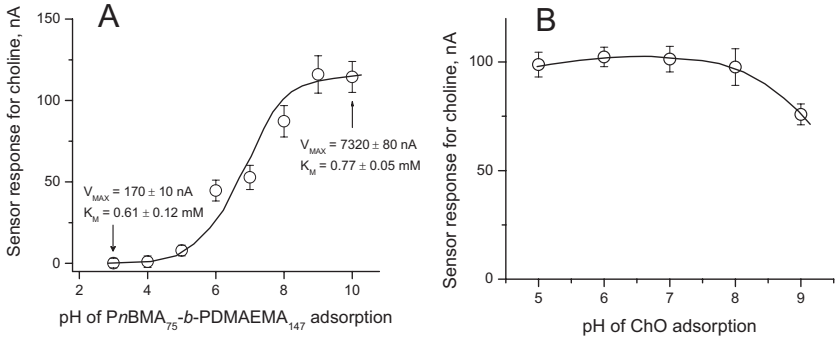

Figure 7. Enzymatic (electrochemical) activity of P*n*BMA$_{75}$-*b*-PDMAEMA$_{147}$/ChO films A) versus the pH of P*n*BMA$_{75}$-*b*-PDMAEMA$_{147}$ adsorption or B) versus the pH of enzyme adsorption. Conditions for (A): adsorption of the diblock copolymer: 10 g L^{-1} P*n*BMA$_{75}$-*b*-PDMAEMA$_{147}$ solution in 50 mM PBS (pH 3–10) for 1 h. Adsorption of ChO: 4 g L^{-1} solution in 10 mM tris (pH 7) for 10 min. Conditions for (B): adsorption of the diblock copolymer: 10 g L^{-1} P*n*BMA$_{75}$-*b*-PDMAEMA$_{147}$ solution in 50 mM PBS (pH 9) for 1 h. Adsorption of ChO: 4 g L^{-1} M solution in 10 mM tris (pH 5–9) for 10 min. The electrochemical (enzymatic) activities of ChO in the films were measured as sensor responses for 10^{-5} M concentration of choline. Lines through the experimentally derived data points are drawn only as a guide to the eye.

the enzyme adsorption. The data on ChO activity in the films are presented in Figure 7. A pronounced increase in the enzymatic activity of the P*n*BMA$_{75}$-*b*-PDMAEMA$_{147}$/ChO films was observed with increasing pH during P*n*BMA$_{75}$-*b*-PDMAEMA$_{147}$ adsorption (Figure 7A), although the low biosensor activities found at pH <5 might also originate from the decrease in the H_2O_2 sensitivity of the MnO_2 layer after exposure to acidic conditions, which has also been reported by others[45] (for details see Figure S4 and Figure S5, Supporting Information). On the other hand, nearly constant enzymatic activities of the P*n*BMA$_{75}$-*b*-PDMAEMA$_{147}$/ChO films were observed with increasing pH during ChO adsorption, with only ca. 25% decrease of the activity at pH 9 (Figure 7B). All data are in a good agreement with the QCM-D experiments.

Apart from the enzymatic activities of the P*n*BMA$_{75}$-*b*-PDMAEMA$_{147}$/ChO films, we examined the specific apparent kinetic parameters of choline oxidation catalyzed by immobilized ChO, more precise the maximum velocity V_{MAX}^{app} and Michaelis constant K_M^{app} from the Michaelis–Menten equation. These parameters were determined from the film activities obtained for different choline concentrations (data not shown here) for two borderline cases, i.e., when the PnBMA-*b*-PDMAEMA/ChO film was formed at low and at high pH of diblock copolymer adsorption (at pH 3 and 10, respectively). The corresponding values of V_{MAX}^{app} and K_M^{app} are given in Figure 7A. The comparison reveals that a considerable difference exists for the values of V_{MAX}^{app}, this difference being comparable to the activity data. Similar values are obtained for K_M^{app} values, both of them being lower than for native ChO (2.95 mM),[33] which is typical for immobilized enzymes. The observed differences in V_{MAX} ($V_{MAX} = E_0 \times k_{cat}$) mainly relates to the increase in active enzyme concentration (E_0) on the surface, although changes in H_2O_2 sensitivity of the MnO_2 layer also have to be taken into account.

Hence, our results strongly suggest that the specific enzymatic activities of the polymer–enzyme films are determined by the amount of adsorbed enzyme, which in turn is controlled by the amount of pre-adsorbed P*n*BMA$_{75}$-*b*-PDMAEMA$_{147}$ and its degree of protonation.

Finally, the most active P*n*BMA$_{75}$-*b*-PDMAEMA$_{147}$/ChO film was formed on the SPE surface when P*n*BMA$_{75}$-*b*-PDMAEMA$_{147}$ and ChO were adsorbed at pH 10 and 7, respectively, and its analytical characteristics with respect to choline were examined and compared to other known choline biosensors designed via electrostatic adsorption/LbL fabrication.

The change in steady-state baseline current observed for the P*n*BMA$_{75}$-*b*-PDMAEMA$_{147}$/ChO biosensor as a function of choline concentration is shown in Figure 8. The obtained choline calibration curve showed a good linearity in a range between 30 nM and 100 μM. The corresponding regression equation is: $Y = (3.75 \times 10^{-3} \pm 3.08 \times 10^{-3}) + (8.55 \pm 0.95) \times X$, $R = 0.99908$, where Y represents the current in μA and X represents the choline concentration in mM. The sensitivity was evaluated to be 175 μA mM^{-1} cm^{-2}. The

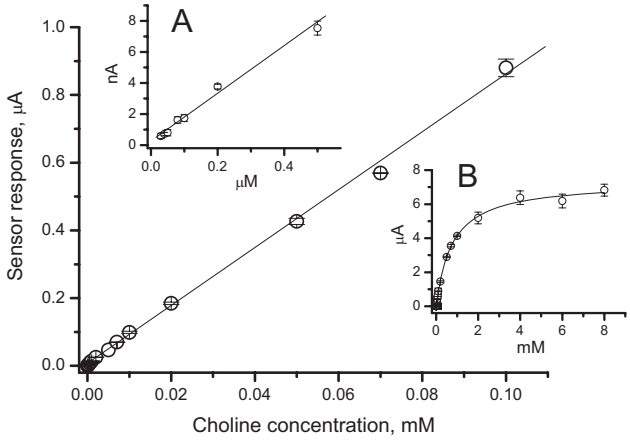

Figure 8. Dependence of steady-state current on the choline concentration for P*n*BMA$_{75}$-*b*-PDMAEMA$_{147}$/ChO biosensor; 50 mM HEPES buffer with 30 mM KCl (pH 7.5), at room temperature. Data are mean ± SD ($n \geq 3$). Linear regression: $Y = (3.75 \times 10^{-3} \pm 3.08 \times 10^{-3}) + (8.55 \pm 0.95) \times X$, $R = 0.99908$, where Y represents the current in μA and X represents the choline concentration in mM. Inserts: A) initial part and B) full range of calibration curve.

Table 3. Comparison of the analytical performance of ChO-based choline biosensors.

Choline biosensor	Type of enzyme attachment	Measuring principle	M_{app} [mM]	Linear range [μM]	Sensitivity [μA mM^{-1} cm^{-2}]	DL [μM]	Refs.
SPE/MnO_2/PnBMA-*b*-PDMAEMA/ChO	Electrostatic adsorption	Amperometry/MnO_2 mediated H_2O_2 oxidation	0.77 ± 0.05	0.03–100	175	0.03	This work
SPE/MnO_2/(PDADMAC/PAS)$_2$/(PDADMAC/ChO)$_3$	LbL	Amperometry/MnO_2 mediated H_2O_2 oxidation	–	0.3–100	103	0.13	[31]
GC/Fe_3PO_4-PB-PDADMAC-ChO	Adsorption	Amperometry/mediated H_2O_2 oxidation	0.47	2–3 200	75	0.4	[48]
GC/(MWCNTs/PANI)$_5$/(PANI/ChO)$_3$-GA	LbL + crosslinking	amperometry/mediated H_2O_2 oxidation	–	1–2 000	0.794	0.3	[49]
GC/ZrO_2-NPs/MWCNTs/(AChE-ChO)	Film casting	Amperometry/mediated H_2O_2 oxidation	–	0.01–200	–	0.01	[50]
Pt/(PEI/ChO)$_{10}$	LbL	Amperometry/H_2O_2 oxidation at Pt	0.436 ± 0.004	0.5–1 000	54	0.5	[51]
Pt/(PDADMAC/ChO)$_8$			0.131 ± 0.003	0.5–100	129	0.5	
Pt-PB/(EACC/ChO)$_{10}$	LbL	Amperometry/H_2O_2 oxidation at Pt	0.083 ± 0.001	0.5–100	89	0.5	[52]
CFE/PPD/AChE-ChO/GA/Naf-MWCNTs	Adsorption + crosslinking	Amperometry/H_2O_2 oxidation	0.52 ± 0.03	0.045–700	–	0.045	[53]
Au/Gs-PBBIns-ChO	Electrostatic adsorption	Chronoamperometry/H_2O_2 oxidation	–	0.1–830	450	0.02	[54]
Pt/ChO-Pluronic F127	Adsorption	Amperometry/H_2O_2 oxidation at Pt	0.228	5–800	8	5	[55]
Pt/(PVS/PAA)$_3$/(ChO/PDADMAC)$_8$	LbL	Amperometry/H_2O_2 oxidation at Pt	–	5–100	177	0.2	[56]
Pt/PDADMAC-ChO-AuNPs-MWCNTs	Electrostatic adsorption	Amperometry/H_2O_2 oxidation at Pt	0.420	1–500	184	0.3	[57]
Au/PtNP-polyCD/ADA/ChO-HRP	Adsorption + immobilization	Square wave voltammetry/HRP mediated H_2O_2 oxidation	–	0.001–10 000	–	0.0001	[58]
Au/CH/GA/Fe_3O_4-NPs/GA/ChO	Adsorption + crosslinking	Square wave voltammetry/HRP mediated H_2O_2 oxidation	–	0.001–10 000	–	0.0001	[59]

AChE, acetylcholinesterase; ADA, adamantan; AuNPs, gold nanoparticles; CFE, carbon fiber electrode; CH, cysteamine hydrochloride; EACC, 6-*o*-ehoxytrimethylammoniochitosan chloride; GA, glutaraldehyde; GC, glassy carbon; HRP, horseradish peroxidase; MWCNTs, multi-walled carbon nanotubes; Naf, nafion; NPs, nanoparticles; PAA, polyallylamine; PANI, poly(aniline); PAS, poly(anethol sulfonate) sodium salt; PB, Prussian blue; PBBIns, poly(*N*-butyl benzimidazole); PDADMAC, poly(diallyldimethylammoniun chloride); PEI, poly(ethylene imine); polyCD, poly(cyclodextrin); PPD, poly(*o*-phenylenediamine); PtNPs, platinum nanoparticles; PVS, poly(vinyl sulfate); SPE, screen-printed electrode.

detection limit at a signal-to-noise ratio (S/N) of 3 was estimated to be 30 nM. The response time was quite rapid: 90% of the steady-state current was achieved within 10 s. Measurements yielded a relative standard deviation (RSD) of 2.7% for >10 determinations of 100 μM of choline. In addition, the P*n*BMA$_{75}$-*b*-PDMAEMA$_{147}$/ChO biosensor retained 80% of its initial current response after two weeks of storage in the dry state at +4 °C.

Table 3 summarizes a detailed comparison of the analytical characteristics of the herein developed biosensor with those reported previously. In most cases, other examples were fabricated by electrostatic adsorption or LbL techniques. From Table 3, it is clearly evident that the analytical performance of our system is highly competitive regarding linearity, sensitivity, and the detection limit for choline. In particular, it should be noted that our fabrication process consists of only two steps and that the best-suited conditions can be chosen for each. No additional improvements regarding conductivity (via application of carbon materials, like multiwalled carbon nanotubes (MWCNTs), nanoparticles, or conductive polymers) or enzyme loading (via multilayered LbL biosensor setups as it has been done by others, Table 3) have been employed here.

Another important analytical parameter of biosensor performance, the operational stability of the herein presented biosensor coatings was evaluated for ≥10 repeated measurements at a fixed choline concentration. It can be quantitatively described as percentual change of the analytical signal per measurement and can be calculated according to the formula: $\Delta I = 100\% \times tgI/I_1$, where *tgI* is the slope of the dependence of the analytical signal on the number of measurement cycles normalized to the initial analytical signal I_1 and given in percent (see explanations given in Figure S6, Supporting Information). According to this quantification, the closer the value of ΔI reaches zero, the higher the stability of the observed biosensor response is.

The value of operational stability found for P*n*BMA$_{75}$-*b*-PDMAEMA$_{147}$/ChO biosensor coatings is $\Delta I = -0.4 \pm 0.03\%$. It is closer to zero than the values of ΔI we have determined earlier for another system comprising a bilayer film of a strong linear polycation (PDADMAC/ChO ($\Delta I = -2.1 \pm 0.1\%$))[46,47] or a multilayer film containing a combination of a strong linear polycation and polyanion ((PDADMAC/PAS)$_2$/(PDADMAC/ChO)$_3$ ($\Delta I = -0.6 \pm 0.2\%$)[31]–(abbreviations of the polyelectrolytes are given in footnotes to Table 3)). At this point, we hypothesize that the nature of the hydrophobic core and the size of the intermediate core–corona micelles both play important roles but to clarify this further studies are required where both nature and weight fraction of the hydrophobic block will be systematically varied.

Finally, as an attempt to further stabilize the biosensor coating, we applied well-known enzyme-to-enzyme crosslinking using GA. Treatment for 1 h with a 1% GA solution already led to significant improvements in ΔI, which was calculated as $+0.08 \pm 0.03\%$ for P*n*BMA$_{75}$-*b*-PDMAEMA$_{147}$/ChO/GA film.

4. Conclusion

We could demonstrate that sequential electrostatic adsorption of P*n*BMA$_{75}$-*b*-PDMAEMA$_{147}$ diblock copolymer micelles and an enzyme ChO leads to well-defined, highly active, and stable biosensor coatings. Thereby, the pH during adsorption of P*n*BMA$_{75}$-*b*-PDMAEMA$_{147}$ and, thus, the charge density within the PDMAEMA segment plays a crucial role and best results are obtained if adsorption is carried out at pH 9–10. Under these conditions, the affinity of the material toward the hydrophobic surface is maximized. We could also show that the subsequent adsorption of ChO and, in turn, the activity of the generated biosensors mainly depends on the amount of pre-adsorbed P*n*BMA$_{75}$-*b*-PDMAEMA$_{147}$ though its charge on the stage of the enzyme deposition also can be important. Finally, we demonstrated that crosslinking of the enzymes within such block copolymer–enzyme films improves the operational stability of the devices.

We plan to expand the herein derived basic principles to other biosensor systems and surface modification processes. We think that our results contribute to a further understanding regarding the bottom-up preparation of advanced biosensor coatings. The same principles should be taken into consideration when more complex surface modification approaches are targeted including carbon nanomaterials, nanoparticles, quantum dots, etc.

Acknowledgements: This research was supported by the Russian Foundation for Basic Research (RFBR 11-03-00712-a), Lomonosov Moscow State University Program of Development, and Lomonosov Moscow State University Post-Genomic Program. L.V.S. and D.V.P. gratefully acknowledge the Deutsche Forschungsgemeinschaft (DFG SCHA1640/5-1 and SCHA1640/6-1) for financial support of their research stays at the Friedrich-Schiller-University Jena. S. Stumpf is gratefully acknowledged for help with contact angle measurements and Prof. Alfred Fahr for access to ζ-potential measurements. F.H.S. and U.G. are grateful to the Thuringian Ministry for Education, Science, and Culture (TMBWK; grants #B514-09051, NanoConSens, and #B515-10065, ChaPoNano) for financial support. F.H.S. further is grateful for a starting independent researcher fellowship from the VCI and thanks Prof. Ulrich S. Schubert for continuous support.

Received: December 30, 2013; Revised: February 24, 2014; Published online: April 17, 2014; DOI: 10.1002/mabi.201300580

Keywords: block copolymers; choline biosensors; choline oxidase; enzyme adsorption; polyelectrolytes; polymer films; surface modification

[1] T. Boudou, T. Crouzier, K. Ren, G. Blin, C. Picart, *Adv. Mater.* **2010**, *22*, 441.
[2] A. Halperin, M. Tirrell, T. P. Lodge, *Adv. Polym. Sci.* **1992**, *100*, 31.
[3] J. Rühe, R. Yano, J. S. Lee, P. Koberle, W. Knoll, A. Offenhausser, *J. Biomater. Sci. -Polym. E* **1999**, *10*, 859.
[4] A. Ulman, *Chem. Rev.* **1996**, *96*, 1533.
[5] J. Sagiv, *J. Am. Chem. Soc.* **1980**, *102*, 92.
[6] G. Decher, J. D. Hong, J. Schmitt, *Thin Solid Films* **1992**, *210*, 831.
[7] G. Decher, *Science* **1997**, *277*, 1232.
[8] F. N. Crespilho, V. Zucolotto, O. N. Oliveira, F. C. Nart, *Int. J. Electrochem. Sci.* **2006**, *1*, 194.
[9] J. Wang, G. D. Liu, M. R. Jan, *J. Am. Chem. Soc.* **2004**, *126*, 3010.
[10] S. Mantha, V. A. Pedrosa, E. V. Olsen, V. A. Davis, A. L. Simonian, *Langmuir* **2010**, *26*, 19114.
[11] F. N. Crespilho, M. E. Ghica, C. Gouveia-Caridade, O. N. Oliveira, C. M. A. Brett, *Talanta* **2008**, *76*, 922.
[12] W. Zhao, J. J. Xu, C. G. Shi, H. Y. Chen, *Langmuir* **2005**, *21*, 9630.
[13] H. B. Shi, Z. X. Zhao, Z. Song, J. D. Huang, Y. Yang, J. Anzai, T. Osa, Q. Chen, *Electroanalysis* **2005**, *17*, 1285.
[14] D. Fiorentino, A. Gallone, D. Fiocco, G. Palazzo, A. Mallardi, *Biosens. Bioelectron.* **2010**, *25*, 2033.
[15] S. Förster, V. Abetz, A. H. E. Müller, *Adv. Polym. Sci.* **2004**, *166*, 173.
[16] J. Cho, J. K. Hong, K. Char, F. Caruso, *J. Am. Chem. Soc.* **2006**, *128*, 9935.
[17] Q. S. Mu, J. R. Lu, Y. H. Ma, M. V. P. de Banez, K. L. Robinson, S. P. Armes, A. L. Lewis, R. K. Thomas, *Langmuir* **2006**, *22*, 6153.
[18] K. Emoto, M. Iijima, Y. Nagasaki, K. Kataoka, *J. Am. Chem. Soc.* **2000**, *122*, 2653.
[19] Z. C. Zhu, S. A. Sukhishvili, *J. Mater. Chem.* **2012**, *22*, 7667.
[20] J. Gensel, I. Dewald, J. Erath, E. Betthausen, A. H. E. Müller, A. Fery, *Chem. Sci.* **2013**, *4*, 325.
[21] G. B. Webber, E. J. Wanless, V. Bütün, S. P. Armes, S. Biggs, *Nano Lett.* **2002**, *2*, 1307.
[22] G. B. Webber, E. J. Wanless, S. P. Armes, Y. Q. Tang, Y. T. Li, S. Biggs, *Adv. Mater.* **2004**, *16*, 1794.
[23] G. B. Webber, E. J. Wanless, S. P. Armes, F. L. Baines, S. Biggs, *Langmuir* **2001**, *17*, 5551.
[24] M. R. Talingting, Y. H. Ma, C. Simmons, S. E. Webber, *Langmuir* **2000**, *16*, 862.
[25] I. W. Hamley, S. D. Connell, S. Collins, *Macromolecules* **2004**, *37*, 5337.
[26] V. M. De Cupere, J. F. Gohy, R. Jérôme, P. G. Rouxhet, *J. Colloid Interface Sci.* **2004**, *271*, 60.
[27] K. Sakai, E. G. Smith, G. B. Webber, M. Baker, E. J. Wanless, V. Bütün, S. P. Armes, S. Biggs, *J. Colloid Interface Sci.* **2007**, *314*, 381.
[28] K. Sakai, E. G. Smith, G. B. Webber, M. Baker, E. J. Wanless, V. Bütün, S. P. Armes, S. Biggs, *Langmuir* **2006**, *22*, 8435.
[29] L. V. Sigolaeva, D. V. Pergushov, C. V. Synatschke, A. Wolf, I. Dewald, I. N. Kurochkin, A. Fery, A. H. E. Müller, *Soft Matter* **2013**, *9*, 2858.
[30] M. S. Gromova, L. V. Sigolaeva, M. A. Fastovets, E. G. Evtushenko, I. A. Babin, D. V. Pergushov, S. V. Amitonov, A. V. Eremenko, I. N. Kurochkin, *Soft Matter* **2011**, *7*, 7404.
[31] E. A. Dontsova, Y. S. Zeifman, I. A. Budashov, A. V. Eremenko, S. L. Kalnov, I. N. Kurochkin, *Sens. Actuators B-Chem.* **2011**, *159*, 261.
[32] M. Junginger, K. Kita-Tokarczyk, T. Schuster, J. Reiche, F. Schacher, A. H. E. Müller, H. Cölfen, A. Taubert, *Macromol. Biosci.* **2010**, *10*, 1084.
[33] T. C. Toyobo enzymes, Ltd, **1996-1997**, pp. 75–77.
[34] H. Ahn, Y. Lee, H. Lee, Y. S. Han, B. S. Seong, D. Y. Ryu, *Macromolecules* **2013**, *46*, 4454.
[35] M. Burkhardt, N. Martinez-Castro, S. Tea, M. Drechsler, I. Babin, I. Grishagin, R. Schweins, D. V. Pergushov, M. Gradzielski, A. B. Zezin, A. H. E. Müller, *Langmuir* **2007**, *23*, 12864.
[36] M. V. Voinova, M. Rodahl, M. Jonson, B. Kasemo, *Phys. Scr.* **1999**, *59*, 391.
[37] A. Schallon, C. V. Synatschke, V. Jérôme, A. H. E. Müller, R. Freitag, *Biomacromolecules* **2012**, *13*, 3463.
[38] A. Schallon, C. V. Synatschke, D. V. Pergushov, V. Jérôme, A. H. E. Müller, R. Freitag, *Langmuir* **2011**, *27*, 12042.
[39] I. Choi, R. Suntivich, F. A. Plamper, C. V. Synatschke, A. H. E. Müller, V. V. Tsukruk, *J. Am. Chem. Soc.* **2011**, *133*, 9592.
[40] F. A. Plamper, M. Ruppel, A. Schmalz, O. Borisov, M. Ballauff, A. H. E. Müller, *Macromolecules* **2007**, *40*, 8361.
[41] G. Ladam, P. Schaaf, F., J. G. Cuisinier, G. Decher, J.-C. Voegel, *Langmuir* **2001**, 17.
[42] N. Welsch, Y. Lu, J. Dzubiella, M. Ballauff, *Polymer* **2013**, *54*, 2835.
[43] D. S. Salloum, J. B. Schlenoff, *Biomacromolecules* **2004**, *5*, 1089.
[44] M. Müller, B. Kessler, N. Houbenov, K. Bohata, Z. Pientka, E. Brynda, *Biomacromolecules* **2006**, *7*, 1285.
[45] B. Xu, M. L. Ye, Y. X. Yu, W. D. Zhang, *Anal. Chim. Acta* **2010**, *674*, 20.
[46] L. Sigolaeva, G. Makhaeva, E. Rudakova, N. Boltneva, M. Porus, G. Dubacheva, A. Eremenko, I. Kurochkin, R. J. Richardson, *Chem.-Biol. Interact.* **2010**, *187*, 312.
[47] I. Kurochkin, M. Gromova, E. Dontsova, L. Sigolaeva, A. Eremenko, E. Evtushenko, I. Budashov, E. Nesterova, O. Grigorkevich, S. Savilov, V. Lunin, in: *Portable Chemical Sensors: Weapons Against Bioterrorism, NATO Science for Peace and Security Series A: Chemistry and Biology* (Ed: D. P. Nikolelis), Springer, Netherlands **2012**, pp. 151–170.
[48] H. Zhang, Y. Yin, P. Wu, C. Cai, *Biosens. Bioelectron.* **2012**, *31*, 244.
[49] F. Qu, M. Yang, J. Jiang, G. Shen, R. Yu, *Anal. Biochem.* **2005**, *344*, 108.
[50] S. Pundir, N. Chauhan, J. Narang, C. S. Pundir, *Anal. Biochem.* **2012**, *427*, 26.
[51] H. Shia, Z. Songa, J. Huanga, Y. Yanga, Z. Zhaoa, J.-I. Anzaib, T. Osab, Q. Chena, *Sens. Actuators B-Chem.* **2005**, *109*, 341.
[52] M. Shin, C. Kwon, S. K. Kim, H. J. Kim, Y. Roh, B. Hong, J. B. Park, H. Lee, *Nano Lett.* **2006**, *6*, 1334.
[53] A. Khan, S. Ab Ghani, *Biosens. Bioelectron.* **2012**, *31*, 433.
[54] H. C. Chen, R. Y. Tsai, Y. H. Chen, R. S. Lee, M. Y. Hua, *Anal. Chim. Acta* **2013**, *792*, 101.
[55] T. Shimomura, T. Itoh, T. Sumiya, F. Mizukami, M. Ono, *Talanta* **2009**, *78*, 217.
[56] X. Qin, H. Wang, X. Wang, S. Li, Z. Miao, M. Huang, Q. Chen, *Mater. Sci. Eng. C* **2009**, *29*, 1453.
[57] X. Qin, H. Wang, H. Wang, Z. Miao, L. Chen, W. Zhao, M. Shan, Q. Chen, *Sens. Actuators B-Chem.* **2010**, *147*, 593.
[58] Z. Zhang, J. Wang, X. Wang, Y. Wang, X. Yang, *Talanta* **2010**, *82*, 483.
[59] Z. Zhang, X. Wang, X. Yang, *Analyst* **2011**, *136*, 4960.